Research Article

Fatih Selimefendigil, Faiza Benabdallah, Kaouther Ghachem, Hind Albalawi, Badr M. Alshammari, and Lioua Kolsi*

Single-channel cooling system design by using perforated porous insert and modeling with POD for double conductive panel

https://doi.org/10.1515/phys-2024-0107
received June 29, 2024; accepted December 09, 2024

Abstract: In this study, a single cooling channel system is suggested for conductive double panel systems. The cooling channel for the vertical component uses perforated porous insert (PP-I) and porous insert (P-I), while cylinders are used in the PP-I case. The permeability of the porous channel (Da between 10^{-5} and 10^{-1}), size of the cylinders (Rc between 0 and 0.25), and location of the PP plate (Yp between 1 and 4.5) are all taken into account when calculating the effectiveness of the cooling system using finite element method. It is found that PP-I can effectively control the vortex size and enhance cooling performance, particularly for vertical plate. Nusselt number is enhanced in the absence of cylinders in the vertical channel by 92% as contrasted to 51% in the presence of cylinders. When cylinders are used for the vertical channel, the temperature drop of 13°C is computed. The flow field noticeably changes when the permeability of the P-I and PP-I is altered. The equivalent temperature increases for P-I and PP-I with setups at Da = 10^{-5} and Da = 10^{-2} are 7.7°C and 4.4°C, respectively. The performance of cooling for the vertical plate is influenced favorably by the higher values of the porous plate's vertical placement. By moving the porous object, it is possible to reduce the temperature by 8°C. For panel surface temperature, a proper orthogonal decomposition (POD)-based reconstruction model with 12 POD modes is used. The POD-based model accurately captures the effects of utilizing P-I and PP-I on the panel temperature.

Keywords: cooling channel, double PV, nanofluids, finite element method, perforated porous

*** Corresponding author: Lioua Kolsi,** Department of Mechanical Engineering, College of Engineering, University of Ha'il, Ha'il City 81451, Saudi Arabia, e-mail: l.kolsi@uoh.edu.sa
Fatih Selimefendigil: Department of Mechanical Engineering, Manisa Celal Bayar University, 45140 Manisa, Turkey, e-mail: fatih.selimefendigil@cbu.edu.tr
Faiza Benabdallah: Department of Industrial Engineering and Systems, College of Engineering, Princess Nourah bint Abdulrahman University, P.O. Box 84428, Riyadh 11671, Saudi Arabia, e-mail: FMbenabdallah@pnu.edu.sa
Kaouther Ghachem: Department of Industrial Engineering and Systems, College of Engineering, Princess Nourah bint Abdulrahman University, P.O. Box 84428, Riyadh 11671, Saudi Arabia, e-mail: kgmaatki@pnu.edu.sa
Hind Albalawi: Department of Physics, College of Sciences, Princess Nourah bint Abdulrahman University (PNU), P.O. Box 84428, Riyadh, 11671, Saudi Arabia, e-mail: hmalbalawi@pnu.edu.sa
Badr M. Alshammari: Department of Electrical Engineering, College of Engineering, Ha'il University, Ha'il City 81451, Saudi Arabia, e-mail: bms.alshammari@uoh.edu.sa

Nomenclature

c_i	mode coefficient
CT	modal contribution
Da	Darcy number
h	heat transfer coefficient
k	thermal conductivity
KR	conductivity ratio
L	channel length
L_p	panel length
Hc	channel height
Nu	Nusselt number
p	pressure
Pr	Prandtl number
Re	Reynolds number
T	temperature
Rc	cylinder size
s	spacing between cylinders
u, v	velocity components
x, y	Cartesian coordinates
Yp	plate location
Greek characters	
α	thermal diffusivity
ν	kinematic viscosity

ρ	density
κ	permeability
ε	porosity
Ψ	POD mode
Subscripts	
c	cold
h	hot
m	average
nf	nanofluid
p	solid particle
Abbreviations	
CC	cooling channel
FEM	finite element method
HT	heat transfer
NCy	no cylinder
P-I	porous insert
PP-I	perforated porous insert
POD	proper orthogonal decomposition
PV	photovoltaic
WCy	with cylinder

1 Introduction

Environmental concerns and energy cost are the main problems for the development of energy-efficient products. Thermal management of energy products becomes an important topic in microelectromechanical systems (MEMs), batteries, and photovoltaic (PV) panels [1–4]. For the equipment to operate safely during electronic cooling, the significant amount of dissipated heat must be evacuated as quickly as feasible. In PV technologies, the cell temperature is directly related to the PV efficiency, and it should be lowered [5]. Different methods have been offered in for thermal management of heat transfer (HT) systems. For HT control, many active, passive, and hybrid approaches are employed. Conductive fins, heat pipes, heat sinks, mini-channels, and jet impingement cooling are some of the preferred methods for thermal management, particularly in solar technology for PVs [6–9]. The cell temperature is reduced more by the active approaches. According to the research by Bahaidarah et al. [10], active cooling techniques offer greater heat flux dissipation than other passive techniques, including using heat pipes and heat sinks. Different cooling solutions for PV systems have been taken into consideration in Hasanuzzaman et al. [11]. Efficiency was increased by 22% when active cooling techniques were applied, but only 15.5% when passive techniques were taken into account.

In cooling applications with micro-channels, porous inserts (P-I) can used for flow and HT control. The fluid-coupled porous systems are encountered in various applications, including packed beds, heat exchangers, electronic cooling, oil production, and blood flow in vessels [12–14]. Many studies have taken porous layers (PLs) in thermal systems into account [15,16]. The impact of PLs on free convection in an open cavity was studied by Miroshnichenko et al. [17]. The size and thickness of the PLs were shown to be useful for controlling the HT. Chamkha et al. [18] performed a numerical study to examine natural convection HT in a porous chamber that was differentially heated and partially stacked vertically. The HT was found to be at its maximum for a crucial PL thickness at Rayleigh number values below 10^5. The use of nanofluid (NF) can increase the efficacy of PL. Several different energy system technologies, including solar, refrigeration, energy storage, and convection, have successfully incorporated NF technology [19–24]. NFs have been taken into consideration in numerous studies of solar power applications [25–27]. In a recent review, Hamzat et al. [28] analyzed the effects of using NFs in different solar energy-harvesting devices. PV systems, evacuated tube solar collectors, solar dishes, and parabolic trough solar collectors are some of the applications. It was noted that NF-assisted systems had the greatest performance improvement, whereas a solar-assisted desalination system produced more freshwater with less energy input. Shah and Ali [29] performed a review work of performance of hybrid NF-based solar system. Comparisons were made with mono-NFs. There have been notable improvements in the solar systems' power output and efficiency. The commercialization of binary NF, stability, and higher pumping power were just a few of the issues that were addressed.

Using NF with porous media offers great advantageous as it has been shown in many studies. Mahdi et al. [30] performed a comprehensive review for the application of convective HT in porous media coupled with NFs. Different thermal boundary conditions, different NF types, and porous media geometric effects were examined utilizing the studies that have been carried out and are available in the literature. It was observed that porous media with NF was well suited for use in real-world HT applications. The NF type was found to affect the overall HT improvement. In another review, Esfe et al. [31] analyzed different studies for convective HT of NFs in porous media considering different flow regimes. They observed an ideal nanoparticle loading in numerous thermal systems. The porosity has a reverse effect on the improvement of HT in a natural convection regime. They came to the additional conclusion that the literature lacked experimental research that examined NF behavior in porous medium.

By utilizing POD (proper orthogonal decomposition) method, cooling performance estimates are obtained. POD is used in the creation of dynamic models, multiphysics and multiparametric HT systems, model order reduction, identification of coherent structures, and flow control [32–36]. Successful application of POD has been achieved for convective HT systems [37–40]. In PV systems, the determination of the spatial variation of temperature on the cell surface is important as the temperature uniformity, and location of hot spots are also important along with the average temperature, which is related to the efficiency of the PV. In this work, a reconstruction-based model with POD is proposed for the fast calculation of the panel surface temperature coupled with single cooling system equipped with P-I and perforated porous insert (PP-I) systems.

In the literature, the utilization of porous object and layers with NFs have been considered in channel cooling applications. In PV, cooling application of porous objects has been considered [41,42]. It has been suggested to use single channels and channels with various inserts to regulate the thermal output of single PVs. However, in actual applications, cooling many PVs should be taken into account with efficient techniques [43]. In this study, for two conductive panels that are oriented at right angles, a unique cooling channel (CC) is developed. The vertical channel's cooling performance decreases when it is used with a single channel, and the inlet flow is parallel to the horizontal channel. Therefore, this channel uses P-I and PP-I to address this issue. Less material is used, and the cooling system will be lighter overall in the CC with PP-I. The cost

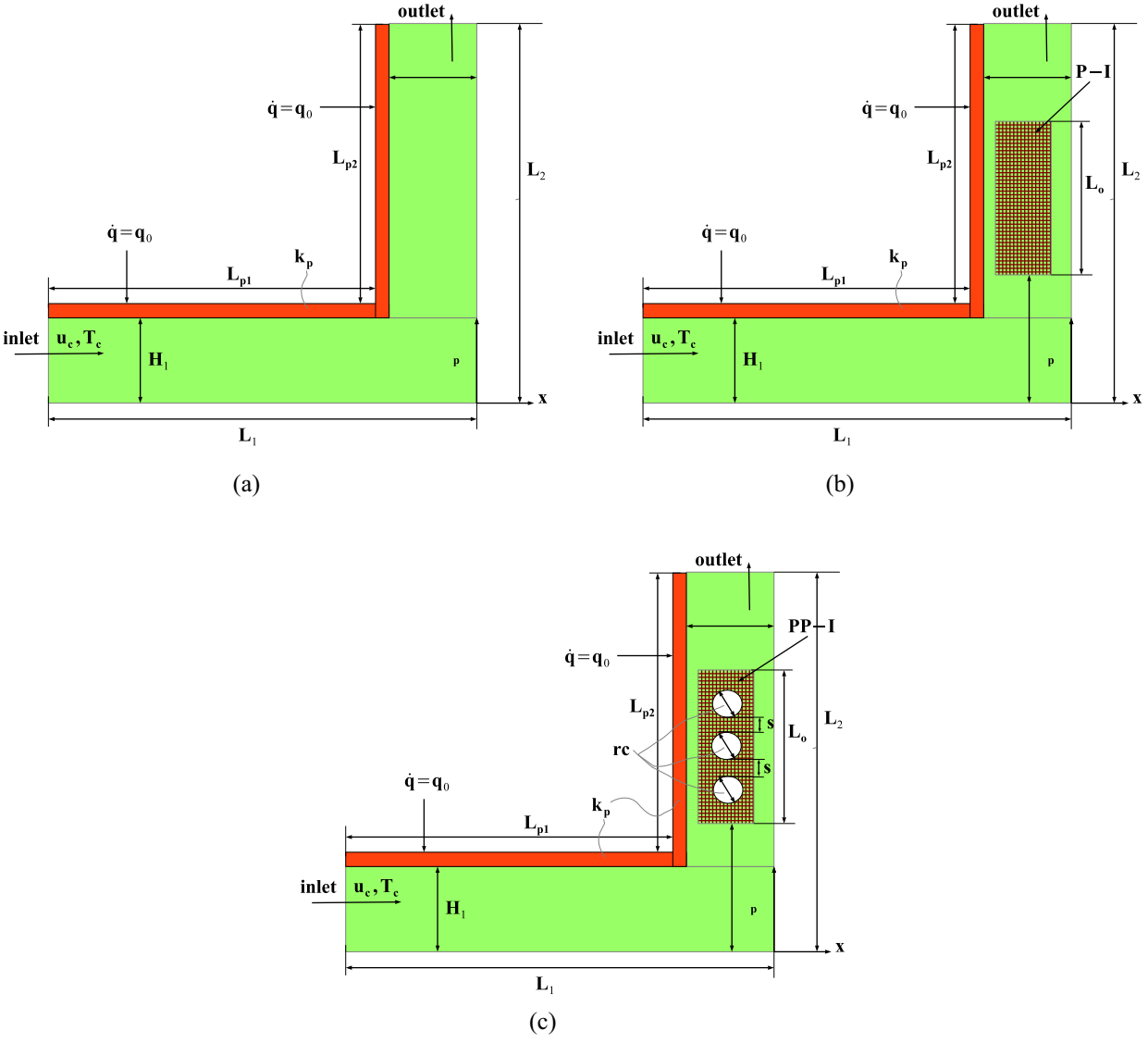

Figure 1: Different CC configurations for double conductive panel systems: (a) SCC, (b) SCC with P-I, and (c) SCC with PP-I.

of the materials will be reduced in addition to the cost of production. The technique is passive, mounting into the CC system is simple, and it does not require external excitation. To the best of authors' knowledge, such an approach of cooling method for two panels by using a single channel having P-I and PP-I has never considered. A prediction method based on POD is utilized for panel temperature reconstruction. The findings and proposed methods based on POD temperature reconstruction are helpful in preliminary design and optimization studies for the development of the cooling system for MEMs, battery modules, and solar panels.

2 Vertically aligned conductive panel system cooled with a single channel

For thermal management of two conductive panels that are arranged vertically, a single cooling channel (SCC) is used. In Figure 1, different CCs are seen. In the second and third channel configurations, as shown in Figure 2(b) and (c), P-I and PP-I are employed. The horizontal and vertical channels are composed of the same materials and have a thermal conductivity of k_p, but their lengths are $L_{p1} = L_{p2} = L_p$. The CCs have lengths of $L_1 = L_2 = L$ and heights of $H_1 = H_2 = H$. The object is positioned in a vertical channel that is L_o in length and H_o in height. Its vertical offset from the bottom is y_p. In the final channel arrangement, identical circular cylinders with radius rc are used to perforate the porous plate. The cylinders are evenly spaced apart on the plate at a spacing of s. The current study makes use of single-phase NF modeling and forced convection of NF. The effects of thermal radiation, viscous dissipation, and natural convection are not taken into consideration. The CCs have a 2D, laminar flow. The generalized Darcy–Brinkmann–Forchheimer extended model for porous zone is taken into consideration in the region of P-I or PP-I.

Conservation equations are expressed as follows based on the presumptions mentioned above [44,45]:

$$\frac{\partial u}{\partial x} + \frac{\partial v}{\partial y} = 0, \tag{1}$$

$$\left(u\frac{\partial u}{\partial x} + v\frac{\partial u}{\partial y}\right) = -\frac{1}{\rho_{nf}}\frac{\partial p}{\partial x} + \nu_{nf}(\nabla^2 u), \tag{2}$$

$$\left(u\frac{\partial v}{\partial x} + v\frac{\partial v}{\partial y}\right) = -\frac{1}{\rho_{nf}}\frac{\partial p}{\partial y} + \nu_{nf}(\nabla^2 v), \tag{3}$$

$$\left(u\frac{\partial T}{\partial x} + v\frac{\partial T}{\partial y}\right) = \alpha_{nf}\nabla^2 T. \tag{4}$$

For the PL of the plate (P-I or PP-I) [44,45]:

$$\frac{\partial u}{\partial x} + \frac{\partial v}{\partial y} = 0, \tag{5}$$

$$\frac{1}{\varepsilon^2}\left(u\frac{\partial u}{\partial x} + v\frac{\partial u}{\partial y}\right) = -\frac{1}{\rho_{nf}}\frac{\partial p}{\partial x} + \frac{\nu_{nf}}{\varepsilon}(\nabla^2 u) - \nu_{nf}\frac{u}{K} - \frac{F_c}{\sqrt{K}}u\sqrt{u^2 + v^2} \tag{6}$$

$$\frac{1}{\varepsilon^2}\left(u\frac{\partial v}{\partial x} + v\frac{\partial v}{\partial y}\right) = -\frac{1}{\rho_{nf}}\frac{\partial p}{\partial y} + \frac{\nu_{nf}}{\varepsilon}(\nabla^2 v) - \nu_{nf}\frac{v}{K} - \frac{F_c}{\sqrt{K}}v\sqrt{u^2 + v^2} \tag{7}$$

$$\left(u\frac{\partial T}{\partial x} + v\frac{\partial T}{\partial y}\right) = \alpha_{nf}\nabla^2 T. \tag{8}$$

For the conductive panels:

$$\nabla^2 T = 0. \tag{9}$$

The following non-dimensional parameters are used:

$$X = \frac{x}{H}, \quad Y = \frac{y}{H}, \quad U = \frac{u}{u_c}, \quad V = \frac{v}{u_c}, \quad P = \frac{p}{\rho_{nf}u_c^2} \quad \theta = \frac{T - T_c}{T_h - T_c}$$
$$\mathrm{F}_c = \frac{1.75}{\sqrt{150\varepsilon^3}}, \quad \mathrm{Pr} = \frac{\nu_f}{\alpha_f}, \quad \mathrm{Re} = \frac{u_c H}{\nu_{nf}}, \quad \mathrm{Da} = \frac{K}{H^2}. \tag{10}$$

The followings can be used to express the governing equations in their non-dimensional form [44]:

$$\frac{\partial U}{\partial X} + \frac{\partial V}{\partial Y} = 0, \tag{11}$$

$$\frac{1}{(\delta_1\varepsilon)^2}\left(U\frac{\partial U}{\partial X} + V\frac{\partial U}{\partial Y}\right) = -\frac{\partial P}{\partial X} + d_1\frac{1}{(\delta_1\varepsilon)\,\mathrm{Re}}(\nabla^2 U) - d_1\frac{U}{\mathrm{DaRe}}\delta_2 - \frac{F_c}{\sqrt{\mathrm{Da}}}U\sqrt{U^2 + V^2}\delta_2, \tag{12}$$

$$\frac{1}{(\delta_1\varepsilon)^2}\left(U\frac{\partial V}{\partial X} + V\frac{\partial V}{\partial Y}\right) = -\frac{\partial P}{\partial Y} + d_1\frac{1}{(\delta_1\varepsilon)\,\mathrm{Re}}(\nabla^2 V) - d_1\frac{V}{\mathrm{DaRe}}\delta_2 - \frac{F_c}{\sqrt{\mathrm{Da}}}V\sqrt{U^2 + V^2}\delta_2, \tag{13}$$

$$\left(U\frac{\partial \theta}{\partial X} + V\frac{\partial \theta}{\partial Y}\right) = d_2\frac{1}{\mathrm{RePr}}\nabla^2\theta. \tag{14}$$

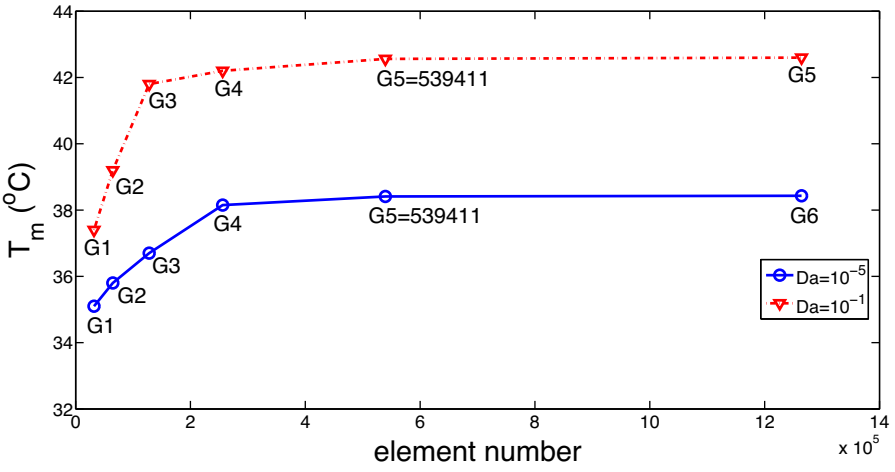

(a)

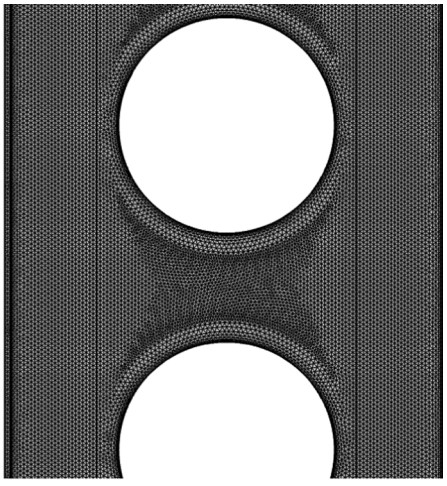

(b)

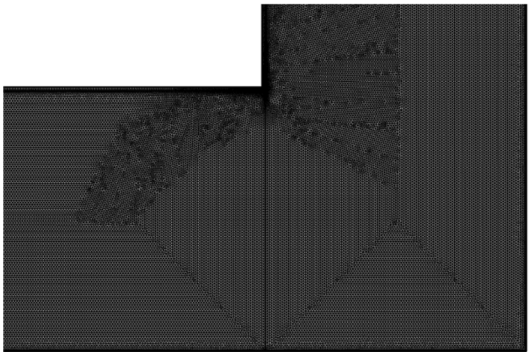

(c)

Figure 2: GIT results for average PST at two different rotational speeds of the first cylinder (a), mesh distribution near the cylinder and panel (b), and near the junction of the channel (c).

where $d_1 = \frac{\nu_{nf}}{\nu_f}$, and $d_2 = \frac{\alpha_{nf}}{\alpha_f}$. For the porous domain, the constants δ_1 and δ_2 are equal to 1, whereas for the NF region, δ_1 and δ_2 are equal to $\frac{1}{\varepsilon}$ and $\delta_2 = 0$, respectively. For the conductive panels:

$$\nabla^2\theta = 0. \tag{15}$$

The boundary conditions are given as:

- At the inlet of SCC:

$$u = u_c \quad \text{and} \quad T = T_c. \tag{16}$$

- At the exit of SCC:

$$\frac{\partial v}{\partial y} = \frac{\partial T}{\partial y} = 0, \quad u = 0. \tag{17}$$

- At the interface between NF and porous object:

$$u_f = u_p, \quad v_f = v_p, k_f\left(\frac{\partial T}{\partial x}\right)_f = k_p\left(\frac{\partial T}{\partial x}\right)_p. \tag{18}$$

- At the interface of the SCC/panel:

$$\left(\frac{\partial T}{\partial n}\right)_f = KR\left(\frac{\partial T}{\partial n}\right)_s, \quad T_f = T_s \tag{19}$$

- At the walls of SCCs:

$$u = v = 0, \quad \frac{\partial T}{\partial n} = 0, \tag{20}$$

- Top wall of the panel:

$$u = v = 0, \quad \dot{q} = q_0. \tag{21}$$

The value of the heat flux is taken as $q_0 = 800\,\mathrm{W/m^2}$.

The following is the balance equation for the PV cell [46]:

$$G(\alpha\tau)_c + G(\alpha\tau)_T(1 - \beta_c) = k_{T1}(T_c - T_g) + k_T(T_c - T_{bs}) + E, \tag{22}$$

where $(\alpha\tau)_c$ and $(\alpha\tau)_T$ represent the cell's and the Tedlar's respective absorbances. The β_c and E variables determine the packing factor and electric output, respectively. Average Nusselt number (Nu) and average panel temperature (T_m) are used to describe the cooling system performance. They are described as:

$$\mathrm{Nu}_s = \frac{h_s D_h}{k}, \quad \mathrm{Nu}_m = \frac{1}{L}\int_0^L \mathrm{Nu}_s \mathrm{d}s, \quad \text{and} \quad T_m = \frac{1}{A_s}\int_0^{A_s} \mathrm{T_s d}A, \tag{23}$$

where the length of plate and panel surface area are L and A_s, respectively, and h_s is the HT coefficient. The following is the local HT:

$$h_x = \frac{\dot{q}}{T_w - T_b}. \tag{24}$$

As for the NF, Al_2O_3-Cu/water NF is used with nanoparticle loading of 0.02 as solid volume fraction. Viscosity and effective thermal conductivity of the NF are obtained using experimentally based measurements in Suresh et al. [47].

The solution is accomplished using the Galerkin weighted residual finite element method (FEM). There are numerous references that discuss the fundamentals and basic modeling processes of utilizing FEM in convective HT [48,49]. The approach uses to approximate the field variable values as [50,51]:

$$u = \sum_{k=1}^{N^u} \Psi_k^{u,v} U_k, \quad v = \sum_{k=1}^{N^v} \Psi_k^{u,v} V_k, \quad p = \sum_{k=1}^{N^p} \Psi_k^{p} P_k, \quad \text{and} \quad T = \sum_{k=1}^{N^u} \Psi_k^{T} T_k, \tag{25}$$

where $\Psi^{u,v}$, Ψ^{p}, and Ψ^{T} are the shape functions. The terms U, V, P, and T indicate the corresponding nodal values. The residual obtained by applying a weight function W is set to zero as follows [50,51]:

$$\int_V WR\mathrm{d}v = 0, \tag{26}$$

by using the W weight function. Instabilities are managed using the streamline upwind Petrov–Galerkin method, and the for the flow and HT modules of the algorithm, biconjugate gradient stabilized (BICGStab) is used. In terms of convergence, a value of 10^{-7} is chosen as the point at which converged solutions are obtained.

It is carried out a mesh independence test investigation. The average panel surface temperature for various grid sizes is shown in Figure 2(a) for two distinct PP-I permeabilities within the CC. For the ensuing calculations, Grid G5, which contains 539,411 elements, is chosen. Figure 2(b) displays the vertical channel of the PP-I's grid distribution. At the intersections of the CC and panel systems and in the direction of the walls, mesh is fine-tuned.

Various research studies that are available in the literature are used for code validation. First validation employed the experimental findings from the study of Young and Vafai [52], which involved the forced convection of both single and numerous objects installed in a channel. They considered Reynolds number between 800 and 13,000. Impacts of channel height, Reynolds number, and heat flux on the thermal performance were investigated. They also validated their results using numerical model. Figure 3(a) compares the Nusselt values for the single object situation at two Reynolds numbers. The difference is found to be 5.5% at Re = 770 and 10.5% at

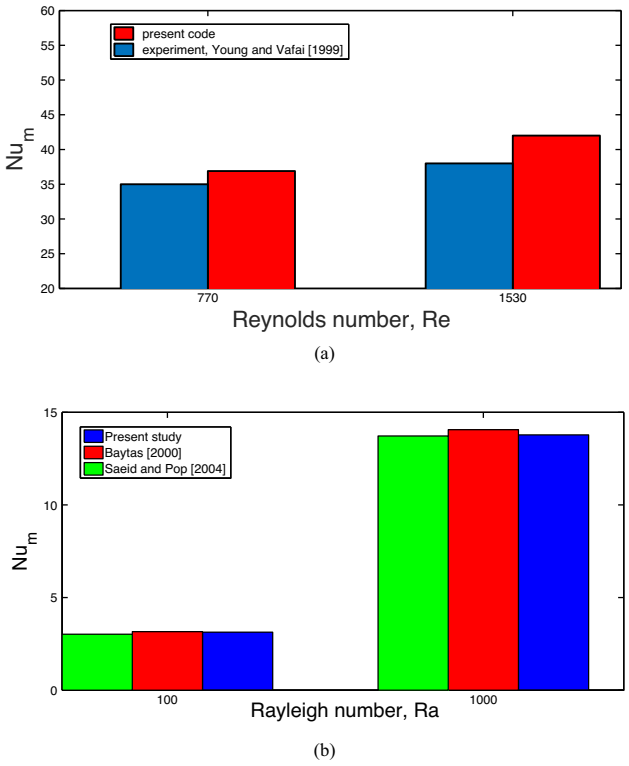

Figure 3: Average Nu comparisons for the mounted blocks in the channel with single object case using the experimental values from the study of Young and Vafai [52] for two distinct values of Reynolds number (a); comparison of the average Nu for HT in a differentially heated porous enclosure at Ra = 100 Ra = 1,000 by using the results in previous studies [53,54] (b).

Re = 1,530. Convection in a heated porous enclosure is taken into consideration in the final validation. Figure 3(b) compares the average Nu values for two different Ra numbers to the literature's various sources [53,54]. For the average Nu, the general agreement is acceptable.

3 Results and discussion

For double conductive panels, an SCC system is proposed. A PP-I is employed in the SCC's vertical portion, while cylinders are used in the rectangular PL. Cooling system effectiveness is numerically evaluated in relation to changes in the Reynolds number (Re between 100 and 500), permeability of the porous channel (Da between 10^{-5} and 10^{-1}), size of the cylinders (RC between 0 and 0.05), and location of the PP plate (yL between 0.2 and 0.9).

For the porous plate with and without cylinders, Figure 4(a)–(f) depicts the effects of Re on the streamline variations. Increases in Re cause the vortices on the corner and the vortex between the plate and upper wall (vertical channel) to grow when there are no cylinders (NCy case). Large vortices are established in the vertical CC behind the porous plate by the placement of the cylinders (WCy case), and when Re rises, their sizes expand. Small vortices are formed on the plate's corner and at the corner junction of the CCs, and their sizes increase with increasing Re. The performance indices of the CCs are average surface temperature and average Nu. As expected, the inclusion of the cylinder in the plate has no effect on the variation of Nu for the horizontal channel, where the increase in average Nu amounts to 50.4% between the highest and lowest Re cases. However, the increase in the Nu becomes 92% when no cylinders are utilized in the vertical channel as opposed to 51% when a cylinder is installed. It is seen that the inclusion of cylinders (PP-I) significantly changes the flow pattern variations within the vertical CC. As the cylinder is used in the porous plate, a large vortex is formed on the top wall at all Re values, which reduces the thermal transport. The increment of the average Nu is lower as compared to case without using cylinders in the plate. The corresponding panel temperature drops become 11.5 °C for the horizontal channel and 20°C (without cylinder). When cylinders are used for the vertical channel, the temperature drop is obtained as 13°C (Figure 4(h)).

The permeability of the porous plate is yet another factor that affects the vertical channel's thermal transport. The variation in plate permeability, as illustrated in Figure 5(a)–(h) for the case with and without cylinders in the porous plate, reveals significant changes in the flow patterns. Lower permeability causes the plate to oppose the flow in the vertical channel more, while vortices are formed on the lower wall of the vertical channel and behind the plate. At Da = 10^{-3}, these vortices disappear while small vortices are formed on the corner and above the plate. When the Da value is at its highest, a sizable recirculation zone forms on the upper wall of the vertical channel as there is only minimal flow resistance. The installation of the inner cylinder of the porous plate results in lower wall vortex formation. When using a cylinder, an upper wall vortex is seen at the maximum Da value, while the bottom wall vortex advances toward the porous plate as the Da value is increased. In terms of average Nu, very slight variations are seen for the horizontal channel as varying the permeability of the plate in the vertical channel. Higher permeability of the plate in the vertical channel generally results in higher Nu values, while the minimum value is attained at Da = 10^{-2}. A lower value of permeability indicates more resistance of the plate to the flow, while only fluid flow is seen in the gap between the plate and upper wall of the vertical channel, which gives higher fluid velocities. On the other hand, for higher permeability, the upper

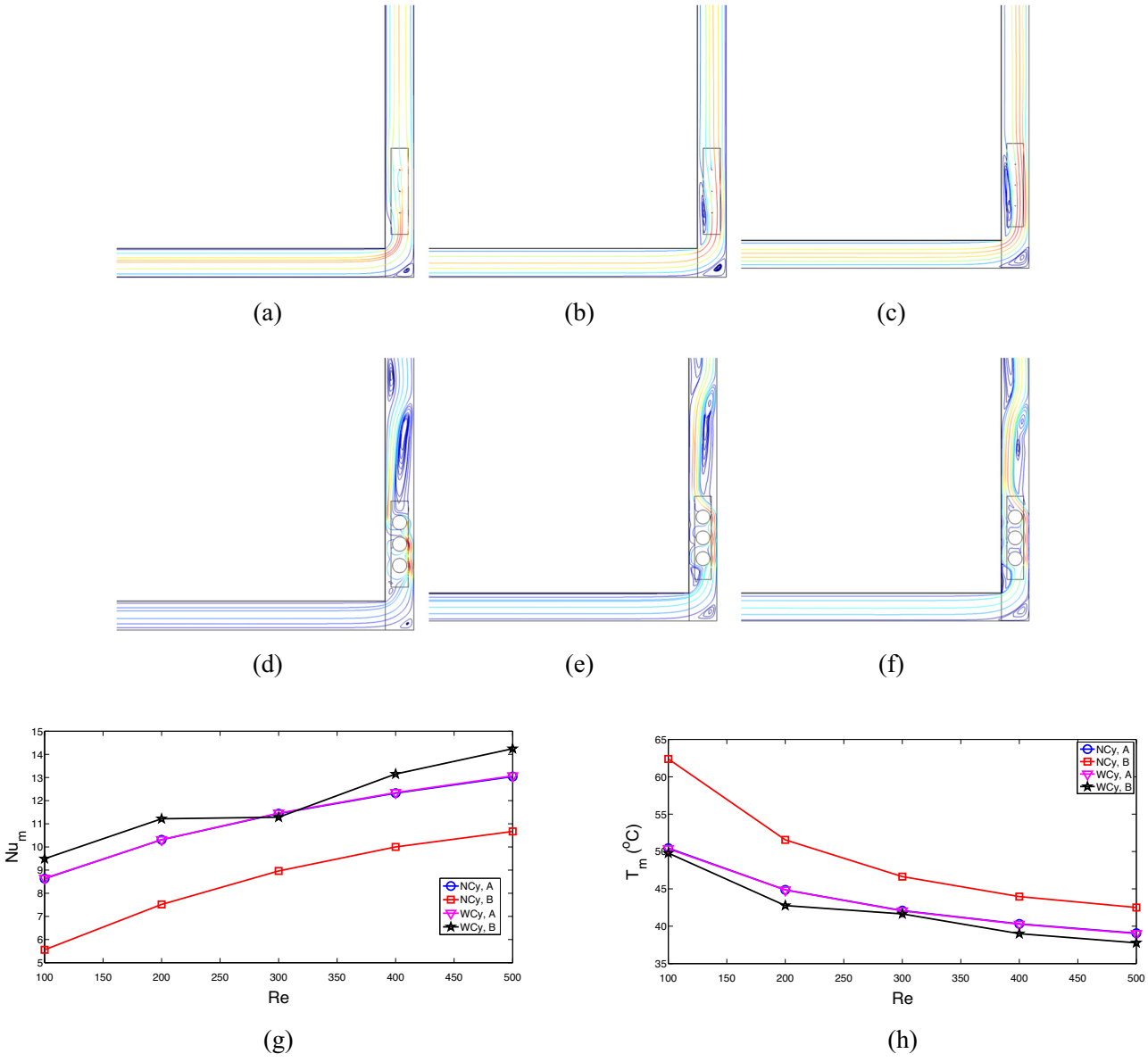

Figure 4: Effects of Re on streamline distributions for P-I (NCy, a–c) and PP-I case (WCy, d–f); impacts of Re on the variation of average Nu (g) and panel surface temperature (h) (Da = 10^{-2}, Rc = 0.25, Yp = 3). (a) NCy, Re = 100, (b) NCy, Re = 300, (c) NCy, Re = 500 (d) WCy, Re = 100, (e) WCy, Re = 300, and (f) WCy, Re = 500.

wall (vertical channel) experiences a large vortex, which has negative impact on the thermal transport and cooling performance. The variation in the average Nu is 16% for plate without cylinder and 7.7% for plate with cylinder when cases at Da = 10^{-5} and Da = 10^{-2} are compared. The corresponding temperature rises are 7.7 °C and 4.4 °C for the cases of NCy and WCy (Figure 5(j)).

Figure 6(a)–(g) illustrates how the streamline variations of the vertical channel depend significantly on the size of the circular cylinder within the porous plate and where the plate is located. A sizable vortex develops on the upper wall (vertical CC) when there is no cylinder (RC = 0). This vortex is disrupted and transferred to the exit of the vertical channel when the size of the cylinders is increased and installed in the porous plate. At the largest size of the cylinders, a sizable bottom wall vortex forms. The top and lower wall vortices of the vertical CC alter in size and location depending on the porous plate's vertical position. In the vertical channel, plate perforation, permeability, and vertical position are effective control mechanisms. The average Nu variation is very slightly affected by the size for the horizontal channel for the vertical channel

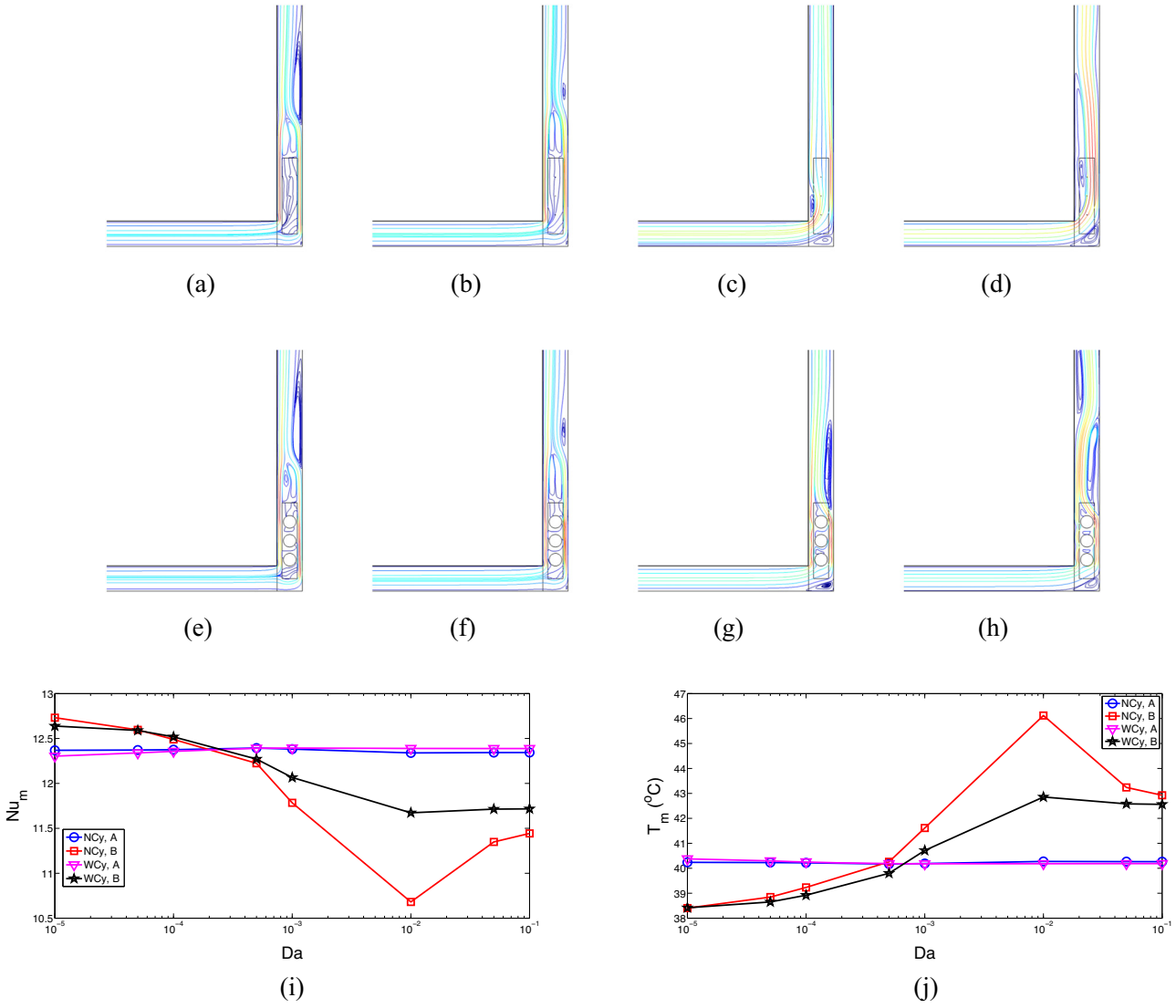

Figure 5: Effects of permeability of the object on the distribution of streamlines for P-I (NCy, a–d) and PP-I (WCy, e–h); impacts of object permeability on the variation of average Nu (i) and average panel temperature (j) (Re = 400, Rc = 0.25, Yp = 3). (a) NCy, Da = 10^{-5}, (b) NCy, Da = 10^{-4}, (c) NCy, Da = 10^{-3}, (d) NCy, Da = 10^{-1} (e) WCy, Da = 10^{-5}, (f) WCy, Da = 10^{-4}, (g) WCy, Da = 10^{-3}, and (h) WCy, Da = 10^{-1}.

with higher permeability. The surface temperature rise is 2.2 °C (Figure 6(i)), and the largest variation of average Nu with cylinder size is obtained as 12%. The cooling performance for the vertical plate is positively impacted by the higher values of the porous plate's vertical placement. With the cylinder installed in the porous plate, the impact becomes greater. When the value of Yp is increased from 1 to 4.5, the average Nu increases by approximately 59% and 27.3%, respectively, for cases with and without cylinders. As a result, the temperatures drop by 8°C (WCy) and 5°C (NCy) (Figure 6(k)).

Finally, different cases are compared in terms of surface temperature drop at Re = 100 (a) and at Re = 500 (b) when the reference cases of panels without cooling are considered. Case 1 denotes the pure fluid (PF) without plate (L-shaped channel only). The best and worst favorable cases are C6 and C3 for horizontal panel. In the best case, NF is used while porous plate with cylinder is installed. There is 2.5 °C temperature difference between the best and worst case at Re = 100 for the horizontal channel. When vertical plate is considered at Re = 100, the worst case is C1 (PF, no-object), while the best case is obtained for C5 (PF, with plate+cylinder). At this condition, NF does not provide the highest cooling rate for the vertical plate. This is due to the establishment vortex within the vertical channel with PF and NF as shown in Figure 7(b) and in Figure 7(c). The vortex in the lower wall of the channel acts as an obstacle, which deflects the fluid toward the

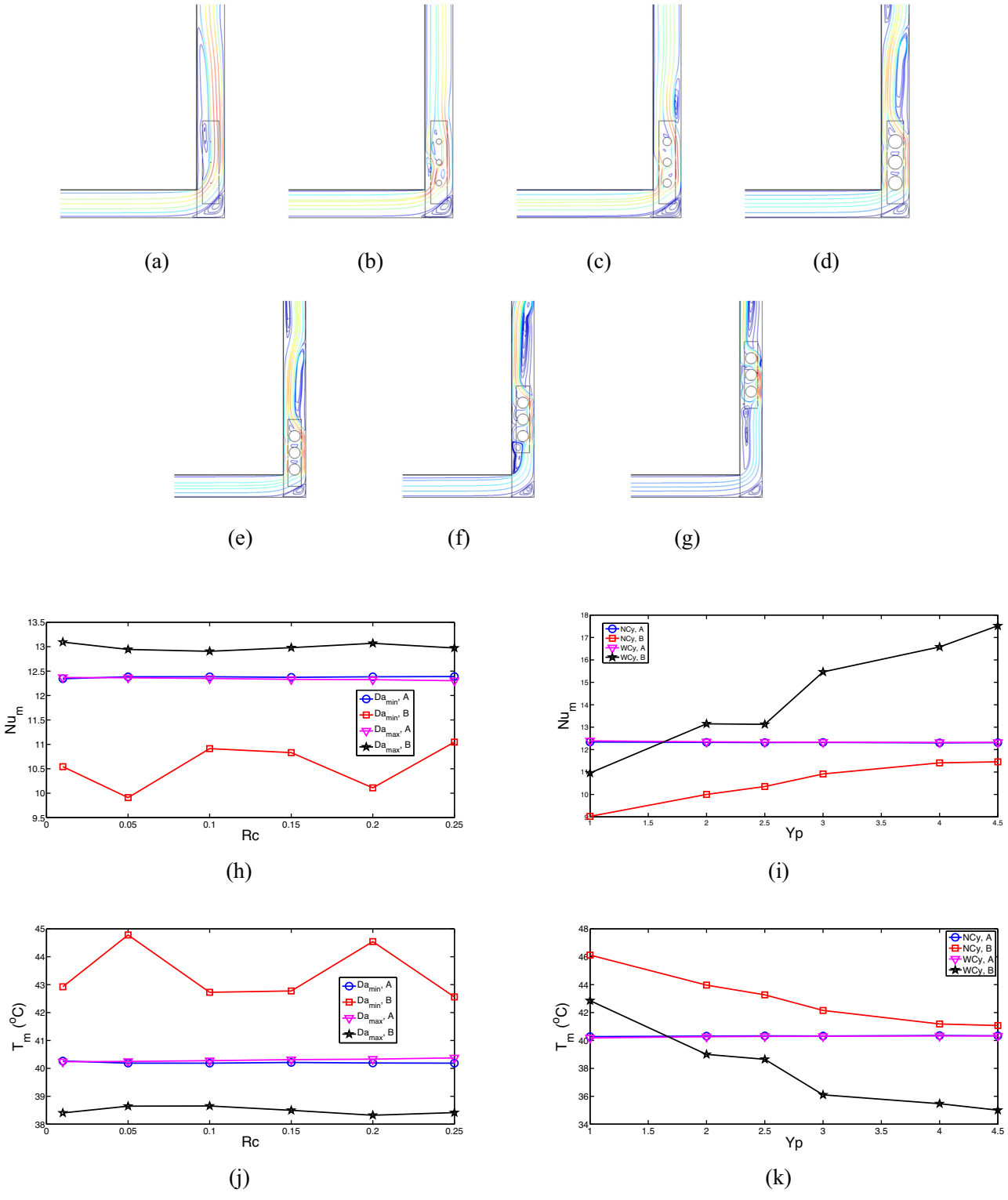

Figure 6: Effects of cylinder size for PP-I (a–d) and porous plate vertical location (e–j) on the streamline variation; average Nu variations with respect to changes in the cylinder size (h) and and porous plate vertical location (i); average surface temperature variations with respect to changes in the cylinder size (j) and and porous plate vertical location (k) (Re = 400, $\mathrm{Da} = 10^{-2}$). (a) Rc = 0, (b) Rc = 0.05, (c) Rc = 0.15, (d) Rc = 0.25, (e) Yp = 1, Rc = 0.25, (f) Yp = 2.5, Rc = 0.25, and (g) Yp = 4.5, Rc = 0.25.

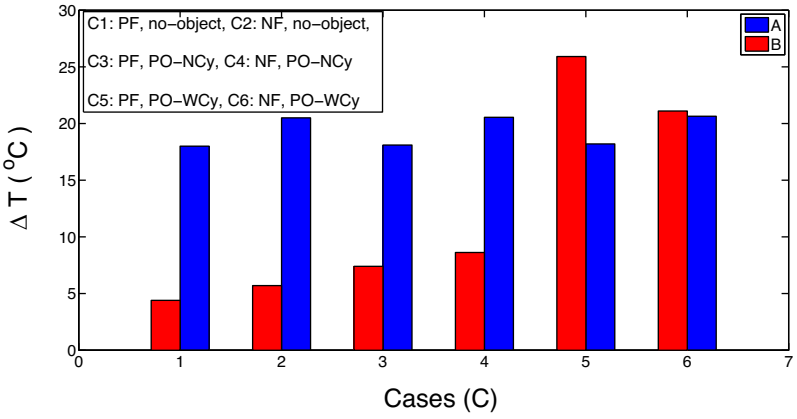

(a)

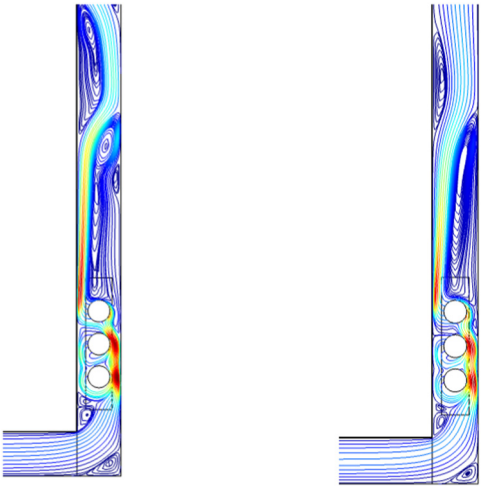

(b) (c)

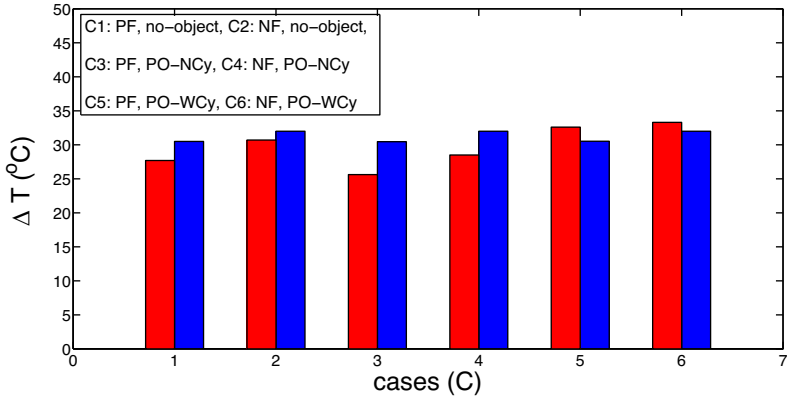

(d)

Figure 7: Comparison of different cases in terms of temperature drop at Re = 100 (a), streamlines for cases C5/C6 (b, c) and comparison of cooling performances at Re = 500 (d).

conductive panel surface and this is effective for the case with using PF instead of NF. Between the NF and PF case, there is 2.2 °C temperature difference. Between the best and worst case of cooling for panel B, there is 21.5 °C temperature difference which shows the effectiveness of using PP-I in the vertical channel for cooling performance enhancement. The NF case for panel A is the best case at Re = 500, with a temperature difference of 1.5 °C between the NF and PF cases. For vertical panel B, the best case is C6 (NF, with plate+cylinder), while the worst one is C3 (PF, plate without cylinder). There is 5. 5°C temperature difference between the cases. PP-I is a useful tool for controlling the vortex size and cooling performance enhancements especially for the vertical plate. Using the PP-I and controlling its permeability, cylinder diameters, and placement in the vertical channel can overcome the drawbacks of using a single cooling system for the double conductive vertically aligned panel system.

3.1 POD-based estimation of vertical panel surface temperature

Average surface temperature estimation of the vertical panel is made by using POD technique. As previously indicated, the POD modeling was considered in numerous

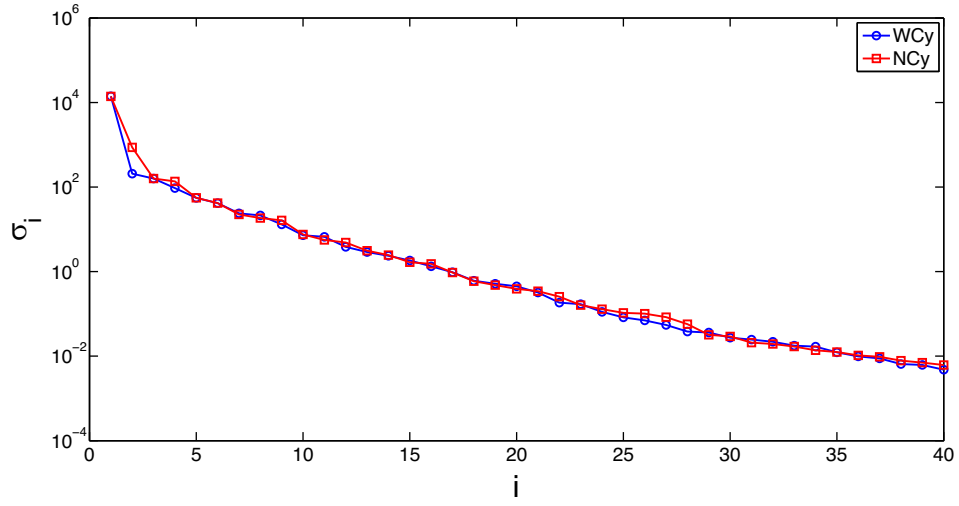

(a)

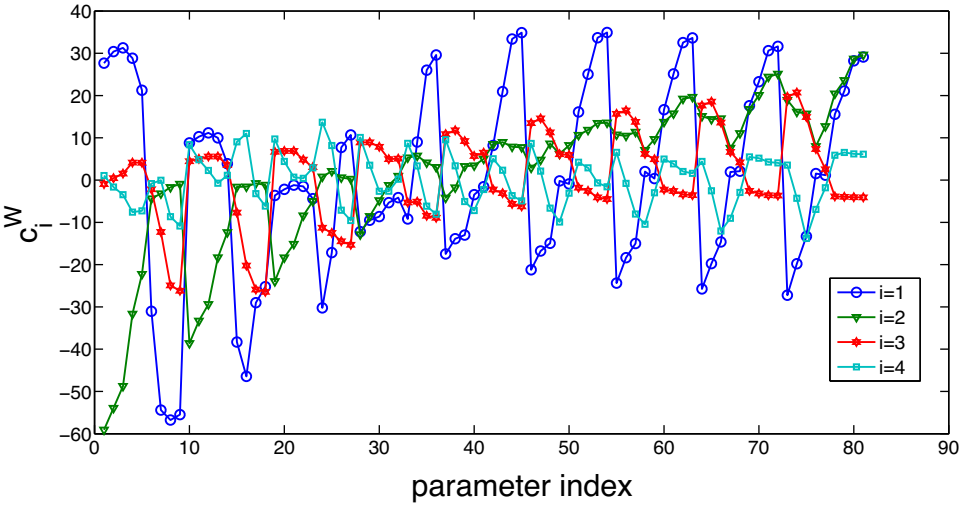

(b)

Figure 8: Variation of singular values for two different cases of P-I (NCy) and PP-I (WCy) (a) and parametric variation of first four mode coefficients for PP-I case (b).

studies on aerodynamic applications, convective HT, flow control, and many other topics. Temperature data from the vertical panel surface are taken in two different configurations. The cases of PP-I and P-I are used. Singular value decomposition is used to obtain the mode coefficients and POD modes from non-dimensionalized data that have been gathered in scalar form. The data (F) are dependent upon the spatial coordinates (x, y) and the parameters (p). It is divided into mean and fluctuating components, the later of which is stated as follows [34]:

$$F = \bar{F} + \sum_{i=1}^{N_m} d_i(p)\Psi(x, y). \tag{27}$$

The number of POD modes is N_m. The following integral eigenvalue problem can be solved to obtain the POD modes [34,40]:

$$\int_V \langle D(\mathbf{x}) \otimes D(\mathbf{x}')\rangle \Psi(\mathbf{x}')d' = \lambda\Psi(\mathbf{x}). \tag{28}$$

Singular value decomposition and the direct technique were both used in this work to determine the POD modes. The POD modes are obtained in a hierarchical manner, with the first mode capturing the majority of the energy and the following modes capturing the second and third largest portions, respectively. It is crucial to mention that POD modeling approach, which has been utilized effectively in numerous research, is applied in this study to obtain the impact of using P-I and PP-I on the cooling performance of the double PV system.

For the domain of the vertical panel system, parametric data with different Reynolds number (Re) and Darcy number (Da) values are gathered. The data set has 4,604 number of spatial points, while 324 number of

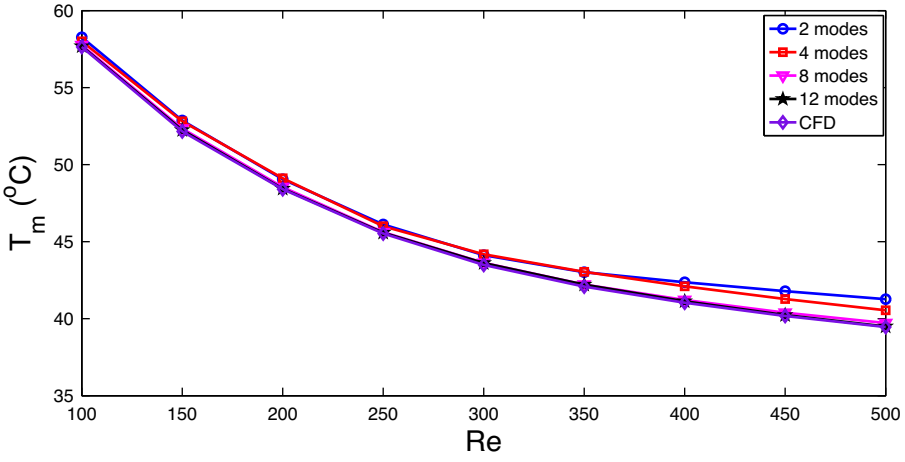

(a)

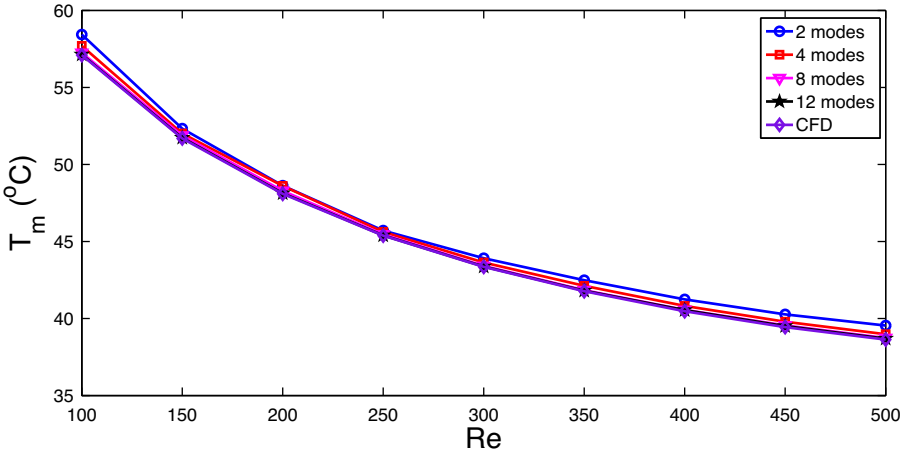

(b)

Figure 9: Comparisons of the reconstructed temperature with varying mode number and for different Re for P-I (NCy) and PP-I (WCy) cases: (a) NCy and (b) WCy.

variations (Re, and Da numbers) are considered. Regarding the Darcy number, 18 various values between 10^{-5} and 10^{-1} are taken into consideration, as well as 18 different values of Re between 100 and 500. In total, 18 × 18 = 324 snapshots make up the entire data set. The POD modes are obtained using singular value decomposition, while modal coefficients can be reproduced by the projecting the data set onto the POD modes as the modes are orthogonal. Considered are two distinct configuration situations. The panel system with P-I and PP-I is used. The contribution (CT) of the modes can be assessed by using the following equation:

$$\mathrm{CT} = \frac{\sum_{k=1}^{N_m}\sigma_k}{\sum_{k=1}^{m}\sigma_k}, \tag{29}$$

where N_m denotes the mode number. The mode number is decided according to CT criteria, which is set to 0.999. The reconstruction of the spatially varying temperature can be done once the modes and parameter-dependent coefficients are obtained. The parametric variation of modal coefficient can be considered, and suitable regression schemes can be used to achieve the modal value at any parametric value in the interval. Once the spatially varying temperature over the surface is found, it is possible to obtain the average, maximum, and minimum of it for the panel surface. The temperature uniformity over the PVs is important to be considered along with the average temperature. The difference between the maximum and minimum temperature can be used as an indication of temperature uniformity over the surface.

The variation of singular values is given in Figure 8(a) for two different cases. In total, 12 modes are used for each of the cases according to the CT criteria. The first mode captures the greatest fraction of the energy, while modal

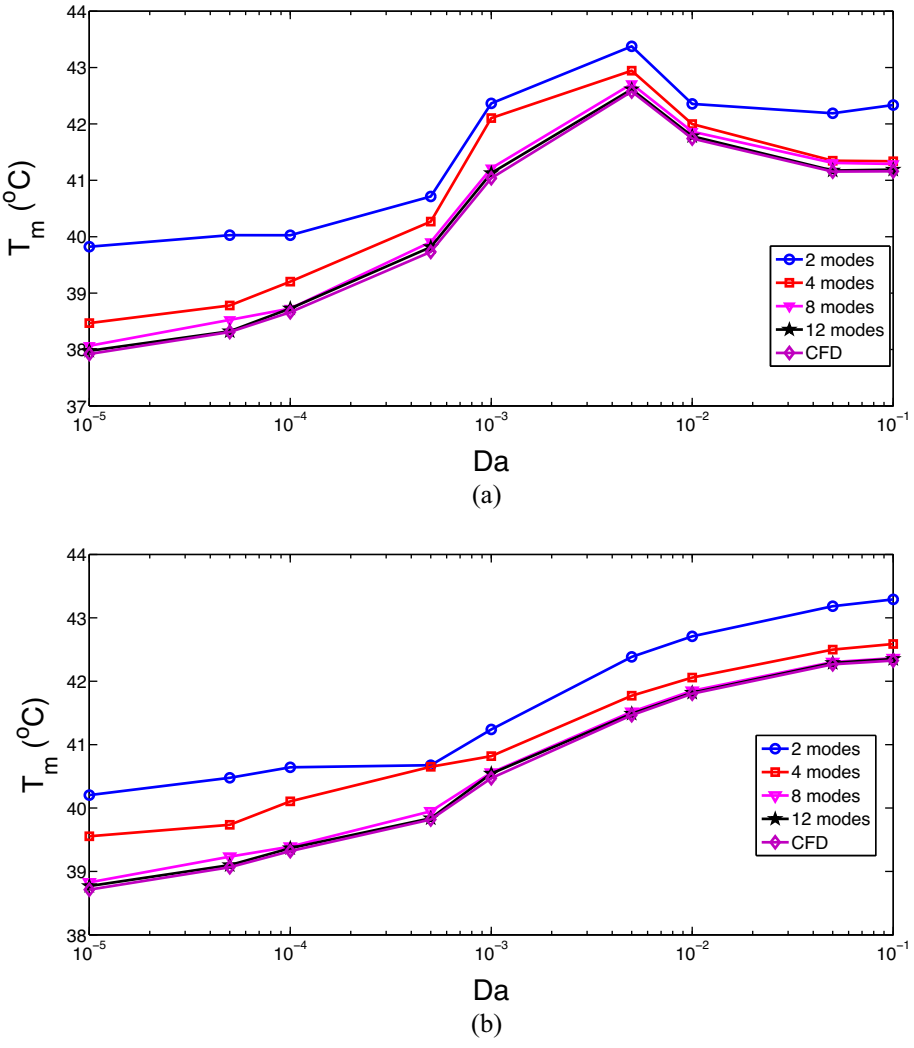

Figure 10: Comparisons of the reconstructed temperature with varying mode number and for different Da for P-I (NCy) and PP-I (WCy) cases: (a) NCy and (b) WCy.

contribution is obtained in a hierarchical way. The parametric variations of first four modes is shown in Figure 8(b) for the case of using PP-I in the CC. Significant variations in the modal coefficients with varying parameters are seen between different modes. The higher-order modal coefficient contribution is higher. As the modes capture the spatial variations, parametric variation is included in the modal coefficient while operating parameters effect the mode coefficients.

The reconstruction of the temperature over the panel surface can be achieved by using modes and modal coefficients. Figure 9 shows the variation of average panel surface temperature with varying Re values for case using P-I and PP-I. When compared to very accurate computational fluid dynamics computations, the trends in the temperature curves with 12 modes are effectively captured. Impacts of permeability of the PP on the change in average temperature are depicted in Figure 10. With the POD-based reconstruction, the different characteristics of utilizing P-I and PP-I on the average panel temperature are clearly captured.

4 Conclusions

This article proposes an SCC for a system of vertically aligned conductive panels. P-I and PP-I are part of the vertical channel, and NF is utilized to boost performance even more. The following significant conclusions can be made:

- When there are no cylinders in the vertical channel, Nu is increased by 92% as opposed to 51% when a cylinder is present. The comparable temperature drop, calculated when cylinders are utilized for the vertical channel, is 13°C.
- When the permeability of the P-I and PP-I is changed, there are noticeable variations in the flow field. When examples at Da = 10^{-5} and Da = 10^{-2} are compared, the variation in the average Nu is 16% for plates without cylinders and 7.7% for plates with cylinders. For the configurations of NCy and WCy, the corresponding temperature increases by varying Da are 7.7 °C and 4.4 °C.
- The higher values of the porous plate's vertical location have a favorable effect on the cooling performance for the vertical plate. The impact is increased when the cylinder is placed inside the porous plate. The average Nu rises by about 59 and 27.3%, respectively, for situations with and without cylinders, when the value of Yp is increased from 1 to 4.5. The outcome is a decline in temperature of 8°C (WCy) and 5°C (NCy).
- Controlling the vortex size and improving the cooling performance, especially for the vertical plate, can be done well by using PP-I.
- The disadvantages of employing a single cooling system for the double conductive vertically aligned panel system can be avoided by using the PP-I and regulating its permeability, cylinder sizes, and positioning in the vertical channel.
- Using 12 POD modes, the temperature over the panel surface can be recreated. The contrasting effects of using P-I and PP-I on the average panel temperature are clearly reflected using the POD-based reconstruction.

Some possible extensions of the study include exergy analysis of the system and inclusion of different thermal boundary conditions such as spatially varying heat flux. Different forms of the SCC such as bifurcating and wavy forms can be considered.

Funding information: This research project was funded by the Deanship of Scientific Research, Princess Nourah bint Abdulrahman University, through the Program of Research Project Funding After Publication, grant No (44- PRFA-P-29).

Author contributions: Fatih Selimefendigil – conceptualization, methodology, software, validation, writing – original draft, writing – review and editing; Faiza Benabdallah – methodology, validation, writing – review and editing; Kaouther Ghachem – conceptualization, methodology, writing – review and editing, supervision; Hind Albalawi – methodology, writing – review and editing, supervision; Badr M. Alshammari – conceptualization, validation, writing – review and editing, supervision Lioua Kolsi – conceptualization, methodology, writing – review and editing, supervision. All authors have accepted responsibility for the entire content of this manuscript and approved its submission.

Conflict of interest: The authors state no conflict of interest.

Data availability statement: All data generated or analyzed during this study are included in this published article.

References

[1] Mahdi JM, Mohammed HI, Talebizadehsardari P. A new approach for employing multiple PCMs in the passive thermal management of photovoltaic modules. Solar Energy. 2021;222:160–74.
[2] Said Z, Ahmad FF, Radwan AM, Hachicha AA. New thermal management technique for PV module using Mist/PCM/Husk: An experimental study. J Cleaner Product. 2023;401:136798.
[3] Al-Rashed AA, Shahsavar A, Entezari S, Moghimi M, Adio SA, Nguyen TK. Numerical investigation of non-Newtonian water-CMC/

CuO nanofluid flow in an offset strip-fin microchannel heat sink: thermal performance and thermodynamic considerations. Appl Thermal Eng. 2019;155:247–58.
[4] Bayrak F, Oztop HF, Selimefendigil F. Experimental study for the application of different cooling techniques in photovoltaic (PV) panels. Energy Conversion Manag. 2020;212:112789.
[5] Shahsavar A, Alwaeli AH, Azimi N, Rostami S, Sopian K, Arící M, et al. Exergy studies in water-based and nanofluid-based photovoltaic/thermal collectors: Status and prospects. Renew Sustainable Energy Rev. 2022;168:112740.
[6] Lu W, Liu Z, Flor JF, Wu Y, Yang M. Investigation on designed fins-enhanced phase change materials system for thermal management of a novel building integrated concentrating PV. Appl Energy. 2018;225:696–709.
[7] Du Y. Advanced thermal management of a solar cell by a nano-coated heat pipe plate: A thermal assessment. Energy Conversion Manag. 2017;134:70–6.
[8] Javidan M, Moghadam AJ. Experimental investigation on thermal management of a photovoltaic module using water-jet impingement cooling. Energy Conversion Manag. 2021;228:113686.
[9] Mohammadpour J, Salehi F, Sheikholeslami M, Lee A. A computational study on nanofluid impingement jets in thermal management of photovoltaic panel. Renew Energy. 2022;189:970–82.
[10] Bahaidarah HM, Baloch AA, Gandhidasan P. Uniform cooling of photovoltaic panels: A review. Renew Sustainable Energy Reviews. 2016;57:1520–44.
[11] Hasanuzzaman M, Malek A, Islam M, Pandey A, Rahim N. Global advancement of cooling technologies for PV systems: A review. Solar Energy. 2016;137:25–45.
[12] Xu HJ, Xing ZB, Wang F, Cheng Z. Review on heat conduction, heat convection, thermal radiation and phase change heat transfer of nanofluids in porous media: Fundamentals and applications. Chem Eng Sci. 2019;195:462–83.
[13] Mahmoudi Y, Hooman K, Vafai K. Convective heat transfer in porous media. Boca Raton: CRC Press; 2019.
[14] Shenoy A, Sheremet M, Pop I. Convective flow and heat transfer from wavy surfaces: viscous fluids, porous media, and nanofluids. Boca Raton: CRC Press; 2016.
[15] Poulikakos D, Kazmierczak M. Forced convection in a duct partially filled with a porous material. J Heat Transfer. 1987;109:653–62.
[16] Gibanov NS, Sheremet MA, Oztop HF, Abu-Hamdeh N. Effect of uniform inclined magnetic field on mixed convection in a lid-driven cavity having a horizontal porous layer saturated with a ferrofluid. Int J Heat Mass Transfer. 2017;114:1086–97.
[17] Miroshnichenko IV, Sheremet MA, Oztop HF, Abu-Hamdeh N. Natural convection of alumina-water nanofluid in an open cavity having multiple porous layers. Int J Heat Mass Transfer. 2018;125:648–57.
[18] Chamkha AJ, Ismael MA. Natural convection in differentially heated partially porous layered cavities filled with a nanofluid. Numer Heat Transfer A Appl. 2014;65(11):1089–113.
[19] Chamkha AJ, Molana M, Rahnama A, Ghadami F. On the nanofluids applications in microchannels: a comprehensive review. Powder Technology. 2018;332:287–322.
[20] Arshad W, Ali HM. Graphene nanoplatelets nanofluids thermal and hydrodynamic performance on integral fin heat sink. Int J Heat Mass Transfer. 2017;107:995–1001.
[21] Baíri A. Experimental study on enhancement of free convective heat transfer in a tilted hemispherical enclosure by using Water-ZnO nanofluid saturated porous materials. Appl Therm Eng. 2019;148:992–8.
[22] Mahian O, Kolsi L, Amani M, Estellé P, Ahmadi G, Kleinstreuer C, et al. Recent advances in modeling and simulation of nanofluid flows-Part I: Fundamentals and theory. Phys Reports. 2019;790:1–48.
[23] Babar H, Ali HM. Airfoil shaped pin-fin heat sink: potential evaluation of ferric oxide and titania nanofluids. Energy Conversion Manag. 2019;202:112194.
[24] Nakharintr L, Naphon P. Magnetic field effect on the enhancement of nanofluids heat transfer of a confined jet impingement in mini-channel heat sink. Int J Heat Mass Transfer. 2017;110:753–9.
[25] Mahian O, Kianifar A, Kalogirou SA, Pop I, Wongwises S. A review of the applications of nanofluids in solar energy. Int J Heat Mass Transfer. 2013;57(2):582–94.
[26] Wahab A, Hassan A, Qasim MA, Ali HM, Babar H, Sajid MU. Solar energy systems-potential of nanofluids. J Molecular Liquids. 2019;289:111049.
[27] Hu G, Ning X, Hussain M, Sajjad U, Sultan M, Ali HM, et al. Potential evaluation of hybrid nanofluids for solar thermal energy harvesting: A review of recent advances. Sustain Energy Tech Assessments. 2021;48:101651.
[28] Hamzat AK, Omisanya MI, Sahin AZ, Oyetunji OR, Olaitan NA. Application of nanofluid in solar energy harvesting devices: A comprehensive review. Energy Conversion Manag. 2022;266:115790.
[29] Shah TR, Ali HM. Applications of hybrid nanofluids in solar energy, practical limitations and challenges: A critical review. Solar Energy. 2019;183:173–203.
[30] Mahdi RA, Mohammed H, Munisamy K, Saeid N. Review of convection heat transfer and fluid flow in porous media with nanofluid. Renew Sustain Energy Rev. 2015;41:715–34.
[31] Esfe MH, Bahiraei M, Hajbarati H, Valadkhani M. A comprehensive review on convective heat transfer of nanofluids in porous media: Energy-related and thermohydraulic characteristics. Appl Therm Eng. 2020;178:115487.
[32] Sirisup S, Karniadakis GE. Stability and accuracy of periodic flow solutions obtained by a POD-penalty method. J Phys D. 2005;202:218–37.
[33] Berkooz G, Holmes P, Lumley JL. The proper orthogonal decomposition in the analysis of turbulent flows. Ann Rev Fluid Mech. 1993;25:539–75.
[34] Hasan N, Sanghi S. Proper orthogonal decomposition and low-dimensional modelling of thermally driven two-dimensional flow in a horizontal rotating flow. J Fluid Mechanics. 2007;573:265–95.
[35] Ostrowski Z, Białecki RA, Kassab AJ. Estimation of constant thermal conductivity by use of proper orthogonal decomposition. Comput Mechanics. 2005;37:52–9.
[36] Samadiani E, Joshi Y. Reduced order thermal modeling of data centers via proper orthogonal decomposition: a review. Int J Numer Methods Heat Fluid Flow. 2010;20(5):529–50.
[37] Selimefendigil F, Polifke W. Nonlinear, proper-orthogonal-decomposition-based model of forced convection heat transfer in pulsating flow. AIAA J. 2014;52(1):131–45.
[38] Samadiani E, Joshi Y. Proper orthogonal decomposition for reduced order thermal modeling of air cooled data centers. J Heat Transfer. 2010;132(7):071402.
[39] Mahapatra PS, Chatterjee S, Mukhopadhyay A, Manna NK, Ghosh K. Proper orthogonal decomposition of thermally-induced flow structure in an enclosure with alternately active localized heat sources. Int J Heat Mass Transfer. 2016;94:373–9.

[40] Selimefendigil F, Öztop HF. Forced convection and thermal predictions of pulsating nanofluid flow over a backward facing step with a corrugated bottom wall. Int J Heat Mass Transfer. 2017;110:231–47.
[41] Selimefendigil F, Benabdallah F, Ghachem K, Albalawi H, AlShammari BM, Kolsi L. Effects of using sinusoidal porous object (SPO) and perforated porous object (PPO) on the cooling performance of nano-enhanced multiple slot jet impingement for a conductive panel system. Propulsion Power Res. 2024;13(2):166–77.
[42] Tahmasbi M, Siavashi M, Norouzi AM, Doranehgard MH. Thermal and electrical efficiencies enhancement of a solar photovoltaic-thermal/air system (PVT/air) using metal foams. J Taiwan Instit Chem Eng. 2021;124:276–89.
[43] Selimefendigil F, El-Sinawi AH, Oztop HF. Optimization of bifurcating channel cooling system for double inclined conductive panel system under inclined magnetic field. Int J Therm Sci. 2023;191:108358.
[44] Siavashi M, Bordbar V, Rahnama P. Heat transfer and entropy generation study of non-Darcy double-diffusive natural convection in inclined porous enclosures with different source configurations. Appl Therm Eng. 2017;110:1462–75.
[45] Khoei A, Sichani AS, Hosseini N. Modeling of reactive acid transport in fractured porous media with the extended-FEM based on Darcy-Brinkman-Forchheimer framework. Comput Geotech. 2020;128:103778.
[46] Ji J, Liu K, Chow Tt, Pei G, He W, He H. Performance analysis of a photovoltaic heat pump. Appl Energy. 2008;85(8):680–93.
[47] Suresh S, Venkitaraj K, Selvakumar P, Chandrasekar M. Effect of Al2O3-Cu/water hybrid nanofluid in heat transfer. Experiment Thermal Fluid Sci. 2012;38:54–60.
[48] Lewis RW, Nithiarasu P, Seetharamu KN. Fundamentals of the finite element method for heat and fluid flow. West Sussex: John Wiley & Sons; 2004.
[49] Reddy JN, Gartling DK. The finite element method in heat transfer and fluid dynamics. Boca Raton: CRC Press; 2010.
[50] Kaluri RS, Basak T. Role of entropy generation on thermal management during natural convection in porous square cavities with distributed heat sources. Chem Eng Sci. 2011;66(10):2124–40.
[51] Ghalambaz M, Mehryan S, Zahmatkesh I, Chamkha A. Free convection heat transfer analysis of a suspension of nano-encapsulated phase change materials (NEPCMs) in an inclined porous cavity. Int J Thermal Sci. 2020;157:106503.
[52] Young T, Vafai K. Experimental and numerical investigation of forced convective characteristics of arrays of channel mounted obstacles. J Heat Transfer. Feb 1999;121:34–42.
[53] Saeid NH, Pop I. Transient free convection in a square cavity filled with a porous medium. Int J Heat Mass Transfer. 2004;47(8–9):1917–24.
[54] Baytas A. Entropy generation for natural convection in an inclined porous cavity. Int J Heat Mass Transfer. 2000;43(12):2089–99.